The dual role of Spn-E in supporting heterotypic ping-pong piRNA amplification in silkworms

Natsuko Izumi[1,†], Keisuke Shoji[1,2,3,†], Lumi Negishi[4], and Yukihide Tomari[1,2*]

[1] Laboratory of RNA Function, Institute for Quantitative Biosciences, The University of Tokyo, Bunkyo-ku, Tokyo 113-0032, Japan.

[2] Department of Computational Biology and Medical Sciences, Graduate School of Frontier Sciences, The University of Tokyo, Bunkyo-ku, Tokyo 113-0032, Japan.

[3] Graduate school of Bio-Applications and Systems Engineering, Tokyo University of Agriculture and Technology, Koganei-shi, Tokyo 184-8588, Japan.

[4] Laboratory of Chromatin Structure and Function, Institute for Quantitative Biosciences, The University of Tokyo, Bunkyo-ku, Tokyo 113-0032, Japan.

*Corresponding author. Tel: +81 3 5841 7839; E-mail: tomari@iqb.u-tokyo.ac.jp

† These authors contributed equally to this work.

Running title: Spn-E facilitates heterotypic ping-pong

Abstract

The PIWI-interacting RNA (piRNA) pathway plays a crucial role in silencing transposons in the germline. piRNA-guided target cleavage by PIWI proteins triggers biogenesis of new piRNAs from the cleaved RNA fragments. This process, known as the ping-pong cycle, is mediated by the two PIWI proteins, Siwi and BmAgo3, in silkworms. However, the detailed molecular mechanism of the ping-pong cycle remains largely unclear. Here, we show that Spindle-E (Spn-E), a putative ATP-dependent RNA helicase, is essential for BmAgo3-dependent production of Siwi-bound piRNAs in the ping-pong cycle and that this function of Spn-E requires its ATPase activity. Moreover, Spn-E acts to suppress homotypic Siwi-Siwi ping-pong, but this function of Spn-E is independent of its ATPase activity. These results highlight the dual role of Spn-E in facilitating proper heterotypic ping-pong in silkworms.

Keywords: BmAgo3/ping-pong cycle/piRNA/Siwi/Spn-E

Introduction

The PIWI-interacting RNA (piRNA) pathway is a widely conserved RNA silencing mechanism against transposable elements (TEs) in the animal germline (Ozata *et al*, 2019; Wang *et al*, 2023). piRNAs are typically 24–31 nt single-stranded RNAs that guide their associated PIWI proteins to complementary target RNAs. While some PIWI proteins induce transcriptional repression in the nucleus (Aravin *et al*, 2008; Kuramochi-Miyagawa *et al*, 2008; Sienski *et al*, 2012), many PIWI proteins function as endoribonucleases and inhibit target expression by endonucleolytic cleavage in the cytoplasm (Brennecke *et al*, 2007; Gunawardane *et al*, 2007; De Fazio *et al*, 2011; Reuter *et al*, 2011).

PIWI-catalyzed target cleavage not only suppresses the target but also produces new piRNAs. In this process, known as the ping-pong cycle, the 3' fragment of PIWI-cleaved target RNA is incorporated into another PIWI as a new piRNA precursor (pre-pre-piRNA) (Ozata *et al*, 2019; Wang *et al*, 2023). The PIWI-loaded pre-pre-piRNA undergoes additional cleavage at a downstream position by another PIWI protein or the endonuclease Zucchini (Zuc, MitoPLD in mice) to become a precursor piRNA (pre-piRNA) (Ozata *et al*, 2019; Gainetdinov *et al*, 2018; Izumi *et al*, 2020). The cleavage by Zuc not only contributes to the pre-piRNA production but also generates the 5' end of a new pre-pre-piRNA from the downstream cleavage fragment, expanding the production of trailing piRNAs to the 3' direction (Mohn *et al*, 2015; Han *et al*, 2015; Ozata *et al*, 2019; Gainetdinov *et al*, 2018). In many species including silkworms, the 3' end of pre-piRNAs is further trimmed by the exonuclease Trimmer (PNLDC1 in mice) and 2'-*O*-methylated by Hen1 (HENMT1 in mice) (Nishimura *et al*, 2018; Ding *et al*, 2017;

Izumi *et al*, 2016; Zhang *et al*, 2017; Horwich *et al*, 2007; Saito *et al*, 2007; Kirino & Mourelatos, 2007). The resulting mature piRNA, in turn, guides its associated PIWI protein to cleave a complementary target RNA, thereby producing a new piRNA precursor from the opposite strand. Because PIWI proteins cleave target RNAs precisely at a position between the 10th and 11th nucleotides of the guiding piRNA, the ping-pong cycle amplifies pairs of piRNAs that have a 10-nucleotide complementary sequence at their 5' ends (Brennecke *et al*, 2007; Gunawardane *et al*, 2007; Aravin *et al*, 2008). A subset of PIWI proteins preferentially binds to piRNAs with uridine at the first nucleotide (1U) (Wang *et al*, 2023), and they produce piRNAs with an adenine bias at the 10th position (10A) by ping-pong amplification due to the nucleotide preference of the PIWI proteins in target cleavage (Wang *et al*, 2014). In silkworms, the ping-pong cycle typically occurs between the two PIWI proteins, Siwi and BmAgo3 (Kawaoka *et al*, 2009; Nishida *et al*, 2015). Siwi-bound piRNAs have a 1U and antisense bias, while BmAgo3-bound piRNAs have a 10A and sense bias (Kawaoka *et al*, 2009; Nishida *et al*, 2015).

Small RNA-guided target cleavage is a common mode of action for the AGO and PIWI clades of Argonaute (Ago) family proteins (Hutvagner & Simard, 2008; Ozata *et al*, 2019). Unlike AGO proteins, however, PIWI proteins are thought to require ATP-dependent helicases for efficient release of cleaved RNA fragments (Nishida *et al*, 2015; Murakami *et al*, 2021). So far, two ATP-dependent DEAD-box RNA helicases, Vasa and DDX43, have been proposed as the factors responsible for releasing cleavage fragments from Siwi and BmAgo3, respectively (Nishida *et al*, 2015; Murakami *et al*, 2021). Vasa-EQ, a DEAD box mutant of Vasa, lacks the ability to release ATP hydrolysis products and therefore freezes the Siwi-to-BmAgo3 ping-pong intermediate complex (called

"Amplifier"), which contains Vasa, piRNA-bound Siwi, BmAgo3, and Qin (Xiol *et al*, 2014).

piRNA pathway components often exhibit distinct patterns of cellular localization. For example, PIWI proteins and many piRNA factors (e.g., BmAgo3 and Vasa) accumulate in phase-separated perinuclear granules called "nuage" (Lim & Kai, 2007; Aravin et al, 2009; Nishida et al, 2015), while other piRNA factors (e.g., Spindle-E [Spn-E] and Qin) localize to another type of cytoplasmic granule known as processing bodies (P-bodies), where RNA degradation enzymes are enriched (Aravin et al, 2009; Chung et al, 2021; Standart & Weil, 2018). In addition, several piRNA processing factors (e.g., Zuc and Trimmer) are located on the mitochondrial surface through their transmembrane domains (Choi et al, 2006; Saito et al, 2010; Patil et al, 2017; Izumi et al, 2016). Their dynamic subcellular compartmentalization and coordinated actions are critical for piRNA biogenesis (Ge et al, 2019; Chung et al, 2021).

Spn-E, a DExH-box RNA helicase that also features a Tudor domain (Gillespie & Berg, 1995; Siomi *et al*, 2010), is a conserved piRNA factor essential for piRNA-mediated TE silencing (Aravin *et al*, 2001; Vagin *et al*, 2006; Shoji *et al*, 2009; Wenda *et al*, 2017; Chen *et al*, 2023). In contrast to its mouse ortholog Tdrd9, which only modestly affects the piRNA expression profile (Shoji *et al*, 2009; Wenda *et al*, 2017), Spn-E is essential for piRNA biogenesis in flies and silkworms (Vagin *et al*, 2006; Lim & Kai, 2007; Malone *et al*, 2009; Nishida *et al*, 2015). In both flies and silkworms, mutations in the ATPase domain of Spn-E fail to support normal piRNA biogenesis and TE silencing (Ott *et al*, 2014; Nishida *et al*, 2015), indicating that ATPase activity is crucial for Spn-E function. Moreover, in *spn-E* mutant flies, Aub and Ago3 are mislocalized from nuage, and the production of both sense and antisense germline

piRNAs is severely compromised (Lim & Kai, 2007; Malone *et al*, 2009), suggesting a defect in the ping-pong cycle. Silkworm Spn-E forms a complex that contains Siwi and Qin but lacks BmAgo3 and Vasa, and the depletion of Spn-E causes a reduction in both Siwi- and BmAgo3-bound piRNAs (Nishida *et al*, 2015). Accordingly, a model has been proposed in which Spn-E acts in the production of Siwi-bound "primary" piRNAs, under the assumption that biogenesis of BmAgo3-bound "secondary" piRNAs depends on the target cleavage by Siwi-bound "primary" piRNAs via ping-pong (Nishida *et al*, 2015). However, the discovery that target cleavage in ping-pong in fact triggers the production of trailing piRNAs has challenged the original definition of "primary" and "secondary" piRNAs (Mohn *et al*, 2015; Han *et al*, 2015; Ozata *et al*, 2019), thereby blurring the specific role of Spn-E in the piRNA biogenesis pathway.

Here, we investigated the role of Spn-E using an ATPase-deficient mutant, Spn-E-EQ (E251Q), in BmN4 cells derived from silkworm ovaries. We observed that Spn-E-EQ forms aggregates distinct from P-bodies together with BmAgo3 and increases the precursors of Siwi-bound piRNAs. Spn-E knockdown (KD) primarily reduced Siwi-bound piRNAs generated by BmAgo3-mediated target cleavage. Wild-type Spn-E, but not the EQ mutant, could partially restore the reduction in BmAgo3-bound piRNAs, suggesting the requirement of the ATPase activity for this function of Spn-E. Unexpectedly, we also found that Spn-E KD enhances Siwi-Siwi homotypic ping-pong independently of its ATPase activity. The necessity of Spn-E for BmAgo3-dependent Siwi-bound piRNA production was further supported by artificial piRNA reporter experiments in BmN4 cells. In contrast, we found no evidence to support the requirement of DDX43 for piRNA biogenesis in cells, even though the recombinant DDX43 protein showed a robust activity to release the cleavage products of BmAgo3 in

vitro. Our results suggest an essential role for Spn-E in facilitating the production of Siwi-bound piRNAs in the canonical heterotypic ping-pong cycle.

Results and Discussion

Siwi knockdown accumulates Spn-E in BmAgo3 complexes

In the ping-pong cycle of silkworms, the 3' cleavage fragments produced by BmAgo3 are loaded into Siwi as a pre-pre-piRNA and vice versa (Kawaoka *et al*, 2009; Nishida *et al*, 2015). When we analyzed immunopurified BmAgo3 complexes from the lysate of Siwi-KD BmN4 cells, we observed remarkable accumulation of two proteins, p160 and p40 (Fig 1A). LC-MS/MS analysis identified p160 as Spn-E, one of the conserved piRNA factors (p40 will be described elsewhere [Izumi *et al*. manuscript in preparation]). In line with the increased physical interaction, Siwi KD caused an accumulation of Spn-E in BmAgo3-containing nuage in BmN4 cells (Fig 1B). In theory, the depletion of Siwi should lead to an accumulation of BmAgo3, which remains bound to its cleavage fragments that cannot be handed over to Siwi (Nishida *et al*, 2020). Accordingly, we speculated that Spn-E functions during the handover process from BmAgo3 to Siwi in the ping-pong cycle and that Siwi KD causes Spn-E to stall at an intermediate step in this process.

ATPase-deficient Spn-E-EQ exhibits increased association with BmAgo3

Spn-E encodes a putative ATP-dependent RNA helicase belonging to the DExH-box family (Gillespie & Berg, 1995), and its ATPase activity is essential for the production of Siwi-bound piRNAs in silkworms (Nishida *et al*, 2015). To determine the process that requires the ATPase activity of Spn-E, we examined the behavior of the ATPase-deficient mutant Spn-E-EQ (E251Q). We previously reported that Spn-E localizes primarily to P-bodies (Chung *et al*, 2021), while a fraction of Spn-E partially localizes

to BmAgo3-containing nuage (Fig 1B). To minimize the effect of endogenous Spn-E, we depleted it using RNAi with double-stranded RNAs (dsRNAs) targeting the *Spn-E* 3' UTR, and complemented the cells with either wild-type Spn-E or the EQ mutant. Wild-type Spn-E exhibited a dotted distribution throughout the cytoplasm, with partial colocalization with BmAgo3-containing nuage in the perinuclear region (Fig 1C). In contrast, Spn-E-EQ formed aberrant aggregates with BmAgo3 (Fig 1C), which was reminiscent of the aggregates formed by Vasa-EQ with BmAgo3 as previously reported (Xiol *et al*, 2014). These results suggest that Spn-E shows increased association with BmAgo3 in Siwi KD or Spn-E-EQ expression. To confirm this, we immunoprecipitated Spn-E-EQ and examined co-precipitated Siwi and BmAgo3. As expected, the EQ mutation of Spn-E reproducibly enhanced its association with BmAgo3 more than that with Siwi, although the *p*-values for the enhancing effects were slightly above 0.05 by *t*-test with Holm correction (Figs 1D and EV1A). Because Spn-E also localizes to P-bodies (Chung *et al*, 2021), we investigated the localization of DDX6, a marker protein for P-bodies, in cells expressing Spn-E-EQ using an anti-DDX6 antibody (Fig EV1B). Although DDX6 was occasionally found near the aggregates of Spn-E-EQ and BmAgo3, it did not overlap with these proteins (Fig EV1C). Thus, the Spn-E-EQ-BmAgo3 aggregates are probably not P-bodies themselves, but a fraction of them may fuse with P-bodies as these aggregates grow. We also examined the localization of Siwi in Spn-E-EQ expressing cells. We found that a fraction of Siwi colocalized with Spn-E-EQ-BmAgo3 aggregates but to a lesser extent compared to BmAgo3 (Fig EV1D). In addition, we observed some Siwi aggregates without Spn-E and BmAgo3 (Fig EV1D). These results suggest that the ATPase-deficient Spn-E-EQ forms an aberrant complex that is stuck with BmAgo3 and possibly with Siwi as well.

Spn-E-EQ reduces mature Siwi-bound piRNAs while accumulating their pre-piRNAs

To examine whether both Siwi and BmAgo3 are contained within the same Spn-E-EQ complex, we performed a tandem IP experiment. We first immunoprecipitated FLAG-tagged Spn-E-EQ, and the purified Spn-E-EQ complex was subsequently subjected to a second immunoprecipitation with an anti-BmAgo3 antibody to detect the co-precipitated Siwi in the presence or absence of RNase treatment. Siwi was co-purified with BmAgo3 in the second IP, and the level was largely unaffected by RNase treatment (Fig EV1E). These results suggest that Spn-E-EQ, BmAgo3, and Siwi form an aberrantly stable complex. Given that both Siwi and BmAgo3 are co-immunoprecipitated with wild-type Spn-E, albeit less strongly than Spn-E-EQ (Figs 1D and EV1A), we speculate that this tertiary complex is formed at least transiently even under normal conditions.

If Spn-E uses its ATPase activity to facilitate the handover process from BmAgo3 to Siwi, the expression of Spn-E-EQ should, in theory, cause an accumulation of RNA fragments cleaved by BmAgo3, which would become pre-pre-piRNAs for Siwi. To explore this possibility, we attempted to detect piR1712 and piR2986, two representative Siwi-bound piRNAs generated by BmAgo3-mediated cleavage, and their precursors in BmN4 cells expressing Spn-E-EQ by northern blotting. Compared to wild-type Spn-E, Spn-E-EQ caused a reduction in mature piR1712 and piR2986 and a concomitant accumulation of longer RNA signals corresponding to the lengths of their pre-piRNAs (Figs 1E and EV1F, G). We also observed slight accumulation of pre-piR484, the precursor of a BmAgo3-bound piRNA, by expressing Spn-E-EQ, but an

accompanying reduction in mature piR484 was not observed (Figs 1E and EV1F, G). In general, pre-pre-piRNAs are cleaved at a downstream position either by Zuc or another piRNA-guided PIWI protein to become pre-piRNAs (Izumi *et al*, 2020). Unlike Zuc-mediated cleavage, downstream cleavage by PIWI proteins can occur before pre-pre-piRNAs are loaded into new PIWI proteins. After PIWI loading, pre-piRNAs are rapidly trimmed to their mature length, making them undetectable (Izumi *et al*, 2020). Therefore, the pre-piRNAs detected here are likely the cleavage products of downstream PIWI proteins prior to being loaded into new PIWI proteins. Taken together, we concluded that Spn-E-EQ inhibits the handover of BmAgo3-cleaved fragments to Siwi.

Spn-E does not have an activity to release Ago3-mediated cleavage fragments

As Spn-E encodes an RNA helicase, it is conceivable that Spn-E has a function to dissociate the cleavage products from BmAgo3 to facilitate their handover to Siwi. However, DDX43, another DEAD-box RNA helicase, has been reported to be the factor responsible for releasing the cleavage fragments of BmAgo3 (Murakami *et al*, 2021). To determine if Spn-E exhibits an activity similar to DDX43, we repeated the previously reported in vitro assay to examine the release of the cleavage fragments from BmAgo3. To distinguish the 5' and 3' cleavage fragments, we prepared a target RNA radiolabeled with ^{32}P at different positions and performed an in vitro target cleavage reaction using immunoprecipitated BmAgo3. After that, we added recombinant Spn-E protein (rSpn-E) or DDX43 protein (rDDX43) to the reaction and monitored the release of the cleavage fragments in the supernatant (Fig EV1H and I). Consistent with the previous report (Murakami *et al*, 2021), rDDX43 released both the 5' and 3' cleavage fragments into the

supernatant (Fig EV1I). However, despite possessing the ATPase activity (Fig EV1J), rSpn-E did not release the cleavage fragments from BmAgo3 (Fig EV1I). Thus, unlike DDX43, Spn-E does not have the releasing activity for BmAgo3-cleaved RNA fragments in vitro.

To compare the effect of DDX43 dysfunction and Spn-E dysfunction on the cellular status of BmAgo3, we expressed the previously reported ATPase-deficient mutant of DDX43, DDX43-D399A (DA), which retains the capacity to bind BmAgo3 (Murakami *et al*, 2021), in BmN4 cells and examined the localization of BmAgo3. In agreement with the previous report (Murakami *et al*, 2021), DDX43 showed dispersed expression patterns in the cytoplasm, with only occasional and partial overlap with BmAgo3-containing nuage (Figs 1B and EV1K). This pattern was also observed with DDX43-DA (Fig EV1K). Unlike Spn-E-EQ, DDX43-DA neither formed aggregates with BmAgo3 nor affected the subcellular distribution of BmAgo3 (Fig EV1K). In addition, the expression pattern of DDX43 was unaffected by either KD of Siwi or expression of Spn-E-EQ (Figs 1B and EV1L). Overall, DDX43 had much less impact on BmAgo3 in BmN4 cells compared to Spn-E.

Depletion of Spn-E decreases the BmAgo3-dependent production of Siwi-bound piRNAs and increases the Siwi-Siwi homotypic ping-pong

We next knocked down Spn-E or DDX43 using two different dsRNAs, respectively (Fig EV2A and B) and examined the impact of KD on piRNA expression. We first analyzed the changes in the expression of piRNAs derived from TEs. While most TEs showed decreased piRNA production in Spn-E KD, a subset of TEs unexpectedly exhibited increased piRNA production (Fig EV2C, top and middle, red dots). In contrast, DDX43

KD caused little or no change in the production of TE-derived piRNAs (Fig EV2C, bottom). Notably, Murakami *et al*. also failed to detect any apparent effects on endogenous piRNAs upon DDX43 KD (Murakami *et al*, 2021). To determine the identity of the increased piRNAs in Spn-E KD, we classified the TE-mapped piRNAs into three groups according to their changes in expression and examined their nucleotide bias for 1U and 10A, which are hallmarks of Siwi- and BmAgo3-bound piRNAs, respectively (Figs 2A and B, and EV2D−F). We found that over half of the decreased piRNAs in Spn-E KD are "1U but not 10A" piRNAs (Figs 2B [RNAi targeting 3' UTR] and EV2F [RNAi targeting CDS]). Moreover, our re-analysis of previously reported Siwi-IP and BmAgo3-IP piRNA libraries revealed that, as expected, these "1U but not 10A" piRNA species are predominantly bound to Siwi and that their putative partner piRNAs in the ping-pong cycle (i.e., complementary piRNAs bearing a 5' 10-nt overlap) are predominantly bound to BmAgo3 in normal BmN4 cells (Fig EV2G, top). Therefore, Spn-E is required for the production of Siwi-bound piRNAs via BmAgo3-mediated target cleavage. On the other hand, most of the increased piRNAs in Spn-E KD had the "1U and 10A" bias (Figs 2B and EV2F). Importantly, the "1U and 10A" piRNAs and their partner piRNAs with 5' 10-nt complementarity were both concentrated in the Siwi-IP (Fig EV2G, bottom), indicating that they are largely produced through a homotypic ping-pong between Siwi-Siwi.

Based on the above observation, we again categorized the TE-mapped piRNAs into three different types: A→S, S→A, and S→S piRNAs (Fig 2C), where "S" and "A" represent Siwi and BmAgo3, respectively, and the arrow indicates the flow of RNA fragments during ping-pong. For example, A→S piRNAs are predominantly bound to Siwi and have partner piRNAs with 5' 10-nt complementarity that are predominantly

bound to BmAgo3 (i.e., they are Siwi-bound piRNAs produced via BmAgo3-mediated target cleavage). On the other hand, S→S piRNAs are predominantly bound to Siwi and are generated mainly through the Siwi-Siwi homotypic ping-pong. We analyzed the change in the relative abundance of each piRNA type in Spn-E KD or DDX43 KD. In agreement with the analysis based on the 1U and 10A biases (Figs 2B and EV2F), A→S piRNAs were decreased, and S→S piRNAs were conversely increased by Spn-E KD (Fig 2D). In contrast, DDX43 KD had no noticeable effect on the relative abundance of any of the groups (Fig EV2H). Thus, Spn-E, but not DDX43, is required for the BmAgo3-dependent production of Siwi-bound piRNAs and for the suppression of Siwi-Siwi homotypic ping-pong.

We next examined the requirement of the ATPase activity of Spn-E for the production of A→S piRNAs and suppression of S→S piRNAs. We constructed small RNA libraries from BmN4 cells, where endogenous Spn-E was knocked down and either wild-type Spn-E or the ATPase-deficient mutant Spn-E-EQ was expressed. Wild-type Spn-E but not the EQ mutant partially recovered the decrease in A→S piRNAs (Fig 2E), suggesting that the ATPase activity of Spn-E is required for A→S piRNA production (Fig 2F). On the other hand, the enhanced production of S→S piRNAs was rescued by the expression of both wild-type Spn-E and the EQ mutant (Fig 2E), indicating that the presence of Spn-E itself, rather than its ATPase activity, is important for repressing the Siwi-Siwi homotypic ping-pong (Fig 2F).

Spn-E but not DDX43 is required for artificial A→S piRNA production

To confirm the requirement of Spn-E for de novo A→S piRNA production, we developed a reporter system that generates an artificial Siwi-bound piRNA, piR484-A

(Figs 3A and EV3A). This reporter RNA has a target site for an abundantly expressed endogenous BmAgo3-bound piRNA and the resulting cleavage product is expected to be loaded into Siwi via the ping-pong cycle. It also contains another downstream target site for an endogenous Siwi-bound piRNA to define the formation of the 3' end of the pre-piRNA; following cleavage at this downstream position by Siwi, 3' end maturation by Trimmer and Hen1 is expected to occur. We co-transfected this reporter plasmid and dsRNAs targeting *Spn-E* or *DDX43* into BmN4 cells, and detected Siwi-bound piR484-A by northern blotting. As expected, the production of piR484-A was reduced by Spn-E KD (Fig 3B). In contrast, DDX43 KD did not affect the production of piR484-A (Fig 3B), even though the DDX43 mRNA level was markedly decreased by KD (Fig EV3B).

We also tested another reporter that has a target site for a *piggyBac* transposon-derived piRNA, which is essentially the same as the artificial Siwi-bound piRNA reporter used in the previous study (Murakami *et al*, 2021), except that it lacks the upstream EGFP sequence (Fig 3C). Unlike the piR484-A reporter, it lacks any specific downstream piRNA target site that can define the 3' end of the pre-piRNA. To ensure that the reporter piRNA is generated even without 3' end processing, we used not only the circular plasmid but also a linearized plasmid that produces a run-off transcript with a defined 3' end. In theory, the reporter RNA transcribed from the circular plasmid is expected to have a > 60 nt sequence and a poly(A) tail downstream of the cleavage site, so the exact mechanism for 3' end processing after Siwi-loading is unclear (Fig 3C, left). On the other hand, the BmAgo3-cleavage product of the reporter RNA transcribed from the linearized plasmid should yield a 30-nt fragment, which is expected to be loaded into Siwi as an artificial piRNA without requiring additional 3' end processing (Fig 3C, right). Similar to the result from the piR484-A system, the production of the artificial

Siwi-bound piRNA was reduced by Spn-E KD but not by DDX43 KD, for both circular and linearized plasmids (Figs 3D and EV3B). These results strongly support the requirement of Spn-E for A→S piRNA production.

To confirm the necessity of Spn-E ATPase activity for artificial Siwi-bound piRNA production, we performed a KD-rescue experiment. We co-transfected the *piggyBac* piRNA reporter plasmid and either the wild-type Spn-E or the EQ mutant-expressing plasmid, under the knockdown of endogenous Spn-E. Consistent with the analysis of endogenous piRNA expression (Fig 2E), wild-type Spn-E but not the EQ mutant rescued the decrease in the artificial Siwi-bound piRNA caused by Spn-E KD (Fig 3E). Similar results were obtained with the piR484-A reporter (Fig EV3C). Taken together, we concluded that the ATPase activity of Spn-E is required for BmAgo3-dependent production of Siwi-bound piRNAs during the ping-pong cycle.

Although Spn-E has long been studied as a conserved piRNA factor, its role in piRNA biogenesis has remained unclear. In this study, we showed that Spn-E is required for the BmAgo3-mediated production of Siwi-bound piRNAs in silkworms. The notable reduction in A→S piRNAs in Spn-E KD (Fig 2D) and the phenotype observed in the EQ mutant (Fig 1) strongly suggest the role of Spn-E in the ping-pong cycle. Since the expression of Spn-E-EQ increases A→S pre-piRNAs (Figs 1E and EV1G), Spn-E is expected to act as an ATPase after target cleavage by BmAgo3 before the handover of the cleaved fragment to Siwi. However, as purified Spn-E did not exhibit an activity release BmAgo3-mediated cleavage fragments in vitro (Fig EV1I), Spn-E is unlikely to directly dissociate the cleaved fragments from BmAgo3. Considering that Spn-E-EQ forms large aggregates with BmAgo3 (Fig 1C), we speculate that Spn-E uses its ATPase

activity to dynamically regulate the dissociation of protein(s) and/or remodeling of the BmAgo3 complex on target RNAs, thereby allowing the handover of BmAgo3-cleaved fragments to Siwi. This action of Spn-E mirrors the previously discussed role of Vasa in the Siwi-to-BmAgo3 handover (Xiol *et al*, 2014). In flies, Spn-E has been implicated in the ping-pong cycle based on its germline-restricted expression and requirement for germline piRNA production (Vagin *et al*, 2006; Lim & Kai, 2007; Malone *et al*, 2009), but its exact site of action has not been determined. Since Siwi and BmAgo3 are orthologs of Aub and Ago3, respectively, fly Spn-E could also function in the heterotypic ping-pong from Ago3 to Aub. In our current study, we knocked down Spn-E only transiently, but a continued reduction in A→S piRNAs should inevitably lead to a decrease in S→A piRNAs in the ping-pong cycle, ultimately causing a collapse of the entire piRNA pathway. This could explain the sterile phenotype of *spn-E* mutants in flies and silkworms (Gillespie & Berg, 1995; Stapleton *et al*, 2001; Chen *et al*, 2023).

Another ATP-dependent helicase, DDX43, was previously reported to be the helicase responsible for the release of cleavage fragments from BmAgo3 (Murakami *et al*, 2021). Indeed, we were able to confirm the reported activity of the recombinant DDX43 protein in vitro (Fig EV1I). However, we found no evidence to support the requirement of DDX43 for A→S piRNA production in cells (Figs 3B and D, and EV2H). Further investigation is needed to clarify the biological role of DDX43.

Unexpectedly, we found that Spn-E KD hyperactivates Siwi-Siwi homotypic ping-pong and that ATPase-deficient Spn-E-EQ can rescue this phenotype (Fig 2D and E). Thus, the presence of Spn-E itself suppresses the homotypic ping-pong of Siwi independent of its ATPase activity. A similar increase in the Aub-Aub homotypic ping-pong has been reported in *qin* mutant flies (Zhang *et al*, 2011). Considering that Spn-E

forms a complex with Qin and Mael and binds to unloaded Siwi (Nishida *et al*, 2015; Namba *et al*, 2022), their binding to empty Siwi may repress Siwi-Siwi homotypic ping-pong. Alternatively, but not mutually exclusively, the observed increase in S→S piRNAs by Spn-E KD may be due to an excess of Siwi proteins that cannot participate in heterotypic ping-pong. In either case, the dual role of Spn-E is critical for supporting the heterotypic ping-pong amplification of piRNAs. On the other hand, our observations are based on a transient knockdown of Spn-E and overexpression of its ATPase mutant, and it is currently unknown whether piRNAs can be produced by the Siwi-Siwi homotypic ping-pong in a complete loss of Spn-E. Of note, our analysis also revealed that the homotypic Siwi-Siwi ping-pong occurs to some extent at the basal level in naive BmN4 cells (Fig EV2G), suggesting that it may have a biological role. Further research is required to understand the mechanistic and functional differences between the heterotypic Siwi-BmAgo3 ping-pong and the homotypic Siwi-Siwi ping-pong.

Materials and Methods

Cell culture, plasmid transfection, and dsRNA transfection in BmN4 cells

BmN4 cells derived from silkworm ovaries were cultured in IPL-41 medium (AppliChem and HyClone) supplemented with 10% fetal bovine serum at 27°C. Sf9 cells were cultured in Sf-900™ II SFM (Thermo Fisher Scientific/Gibco) at 28°C on an orbital shaker set at 135 rpm. For immunoprecipitation experiments, a total of 4.5–6 μg of plasmid and dsRNA were transfected into BmN4 cells (~2×10^6 cells per 10 cm dish) with X-tremeGENE HP DNA Transfection Reagent (Merck Millipore/Roche). The second transfection was performed 3 days after the first transfection and the cells were harvested after an additional 5 days. For immunofluorescence experiments, a total of 0.4–0.5 μg of plasmid and dsRNAs were transfected into BmN4 cells (4–6 $\times 10^4$ cells per glass bottom 35 mm dish) with X-tremeGENE HP DNA Transfection Reagent (Merck Millipore/Roche), and the cells were fixed 5–6 days later. For artificial piRNA reporter experiments, a total of 3–5 μg of plasmid and dsRNA were transfected into BmN4 cells (~2×10^6 cells per 10 cm dish) with X-tremeGENE HP DNA Transfection Reagent (Merck Millipore/Roche). Transfection was repeated 2 days and 5 days after the first transfection and the cells were harvested after an additional 4 days. For library preparation, a total of 5 μg of plasmid and dsRNA were transfected into BmN4 cells (8 $\times 10^5$ cells per 10 cm dish) with X-tremeGENE HP DNA Transfection Reagent (Merck Millipore/Roche) every 3 days four times. dsRNA preparation was described previously (Izumi *et al*, 2020). Template DNAs were prepared by PCR using primers containing the T7 promoter, as listed in Table EV1.

Plasmid construction

pIExZ-FLAG-Spn-E was described previously (Chung *et al*, 2021). pIExZ-FLAG-Spn-E-E251Q was generated by site-directed mutagenesis.

pIEx-FLAG-DDX43, pIExZ-HA-DDX43

A FLAG-tagged or HA-tagged cDNA fragment of DDX43 was amplified by RT-PCR from total RNA extracted from silkworm ovaries and cloned into the pIEx-1 vector (Merck Millipore/Novagen) or the pIExZ vector using an In-Fusion cloning kit (Takara).

pCold-DDX43, pCold-DDX6

A DNA fragment encoding DDX43 or DDX6 was amplified by PCR and inserted into the pCold-I vector (Takara) using an In-Fusion cloning kit (Takara).

pFastBac-6HFLAGSBP-Spn-E-WT, E251Q

A DNA fragment coding Spn-E-WT or E251Q was amplified by PCR and subcloned into the pcDNA5/FRT/TO vector (Thermo Fisher Scientific) with the FLAGSBP sequence inserted. Then, a DNA fragment encoding 6HisFLAGSBP-Spn-E-WT and E251Q was amplified by PCR and inserted into the pFastBac vector (Thermo Fisher Scientific) using an In-Fusion cloning kit (Takara).

pIEx4-piR484-A reporter

Synthesized DNA oligos with chimeric target sequences of piR484 and piR2986 were annealed (see Fig EV3A) and inserted into the BamHI and HindIII sites of the pIEx4 vector (Merck Millipore/Novagen).

pIB-piggyBac piRNA reporter

The *piggyBac* piRNA target site was inserted into the middle of the V5 coding sequence in the pIB-V5/His vector (Thermo Fisher Scientific) by site-directed mutagenesis. For linearization, the plasmid was digested with *AgeI*, which cleaves 20 bp downstream of

the *piggyBac* piRNA target site (see Fig 3C).

The sequences of primers used for plasmid construction are listed in Table EV1.

Antibodies and western blotting

Rabbit anti-Siwi, anti-BmAgo3, anti-Spn-E, and biotinylated BmAgo3 antibodies were described previously (Izumi et al. 2020,2022). A rabbit anti-DDX6 antibody was generated by immunizing N-terminally His-tagged full-length DDX6. Anti-FLAG (M2, Merck Millipore/Sigma), anti-DYKDDDDK peroxidase conjugated (Wako), anti-HA (3F10, Merck Millipore/Roche), and anti-α-Tubulin (B-5-1-2, Merck Millipore/Sigma) antibodies were purchased. Chemiluminescence was induced by Luminata Forte Western HRP Substrate (Merck Millipore) or SuperSignal™ West Femto Maximum Sensitivity Substrate (Thermo Fisher Scientific), and images were acquired by an Amersham Imager 600 (Cytiva).

Immunoprecipitation

For BmAgo3 immunoprecipitation, cells were resuspended in buffer A [25 mM Tris-HCl (pH 7.6), 150 mM NaCl, 1.5 mM $MgCl_2$, 0.2% sodium deoxycholate, 0.1% lithium dodecyl sulfate, 0.4% NP-40, 0.5 mM DTT, 1 × Complete EDTA-free protease inhibitor (Merck Millipore/Roche), 1 × PhosSTOP (Merck Millipore/Roche)] and incubated on ice for 20 min. The cell suspension was centrifuged at 17,000 × g for 30 min at 4°C, and the cleared lysate was diluted with an equal volume of buffer A without detergents. The cell lysate was incubated with normal rabbit IgG (Cell Signaling Technology) or an anti-BmAgo3 antibody at 4°C for 1 h, and then Dynabeads Protein G (Thermo Fisher Scientific/Invitrogen) was added. After incubation at 4°C for 1.5 h, the beads were

washed five times with buffer A without protease inhibitors and phosphatase inhibitors, and the immunopurified complex was eluted with SDS sample buffer. For FLAG-Spn-E immunoprecipitation, cells were resuspended in buffer B [25 mM Tris-HCl (pH 7.6), 150 mM NaCl, 1.5 mM $MgCl_2$, 0.25% Triton X-100, 0.5 mM DTT, 1 × Complete EDTA-free protease inhibitor (Merck Millipore/Roche), 1 × PhosSTOP (Merck Millipore/Roche)] and homogenized with a Dounce homogenizer on ice. The cell lysate was centrifuged at 17,000 × g for 30 min at 4°C, and the supernatant was incubated with Dynabeads Protein G (Thermo Fisher Scientific/Invitrogen) pre-conjugated with an anti-FLAG antibody (M2; Merck Millipore/Sigma) at 4°C for 1.5 h. The beads were washed five times with buffer C [25 mM Tris-HCl (pH 7.4), 150 mM NaCl, 1.5 mM $MgCl_2$, 0.5% Triton X-100, 0.5 mM DTT], and the immunopurified complexes were eluted with 3X FLAG peptide (Merck Millipore/Sigma). For the tandem IP experiment, the eluate was diluted with an equal volume of buffer D [30 mM HEPES-KOH (pH 7.4), 100 mM KOAc, 2 mM $Mg(OAc)_2$, 0.5 mM DTT]. One-third of the lysate was incubated with normal rabbit IgG (Cell Signaling Technology) and the remaining was incubated with anti-BmAgo3 antibody at 4°C for 30 min, and then Dynabeads Protein G (Thermo Fisher Scientific/Invitrogen) was added. After incubation at 4°C for 1.5 h, the beads were washed five times with buffer C. The BmAgo3 immunoprecipitated beads were divided into two and incubated in buffer D with or without 200 μg/ml RNase A (Qiagen) at 30°C for 15 min. The beads were washed twice with buffer D, and the immunopurified complex was eluted with SDS sample buffer. For Siwi immunoprecipitation in artificial piRNA reporter experiments, cells were resuspended in buffer B and homogenized with a Dounce homogenizer on ice. The cell lysate was centrifuged at 17,000 × g for 30 min at 4°C. The supernatant was further supplemented

with Triton X-100 (final concentration, 1%) and incubated with an anti-Siwi antibody at 4°C for 1 h, and then Dynabeads Protein G (Thermo Fisher Scientific/Invitrogen) was added. After incubation at 4°C for 1.5 h, the beads were washed five times with buffer E [25 mM Tris-HCl (pH 7.4), 150 mM NaCl, 1.5 mM $MgCl_2$, 1% Triton X-100, 0.5 mM DTT]. A portion of the immunopurified complexes was eluted with SDS sample buffer, and the remainder was eluted with TRI Reagent (Molecular Research Center) for northern blot analysis.

Purification of recombinant proteins

pCold-DDX43 and pCold-DDX6 were transformed into Rosetta 2 (DE3) competent cells (Merck Millipore/Novagen). The cells were cultured at 37°C until the OD_{600} reached ~0.6, and then cooled on ice for 30 min. Protein expression was induced with 1 mM IPTG at 15°C overnight. The cell pellets were resuspended in His purification buffer [50 mM HEPES-KOH (pH 7.4), 300 mM NaCl, 13 mM imidazole, 0.2 mM TECP, 10 μg/ml leupeptin, 10 μg/ml aprotinin, 1 μg/ml pepstatin A, 1 × Complete EDTA-free protease inhibitor cocktail (Merck Millipore/Roche)] and sonicated with Bioruptor II (CosmoBio). The cell lysate was centrifuged at 17,000 × g at 4°C for 20 min. The cleared lysate was added to cOmplete His-Tag Purification Resin (Merck Millipore/Roche) and incubated at 4°C for 1.5 h. After the resin was washed with the His purification buffer, the bound proteins were eluted with elution buffer [50 mM HEPES-KOH (pH 7.4), 150 mM NaCl, 300 mM imidazole, 0.2 mM TECP]. The peak fractions were pooled and dialyzed with PBS overnight. 6HisFLAGSBP-Spn-E (WT or E251Q) was expressed in SF9 cells by the Bac-to-Bac Baculovirus Expression system (Thermo Fisher Scientific/Invitrogen). The SF9 cells were resuspended in buffer F [25

mM Tris-HCl (pH 7.4), 150 mM NaCl, 1.5 mM $MgCl_2$, 0.5% Triton X-100, 0.4% NP-40, 1 mM DTT, 1 × Complete EDTA-free protease inhibitor (Merck Millipore/Roche), 1 × PhosSTOP (Merck Millipore/Roche)] and homogenized with a Dounce homogenizer. The cell homogenate was centrifuged at 17,000 × g for 30 min at 4°C. The supernatant was supplemented with Triton X-100 (1%, final concentration), NaCl (450 mM, final concentration), and RNaseA (150 μg/ml, final concentration; Qiagen) and incubated with Streptavidin Sepharose High Performance (Cytiva) at 4°C for 2 h. The Sepharose beads were washed with buffer G [25 mM Tris-HCl (pH 7.4), 550 mM NaCl, 1.5 mM $MgCl_2$, 1% Triton X-100, 0.4% NP-40, 1 mM DTT] and rinsed with buffer H [25 mM Tris-HCl (pH 7.4), 150 mM NaCl, 1.5 mM $MgCl_2$, 0.05% Triton X-100, 1 mM DTT]. The 6HisFLAGSBP-Spn-E (WT or E251Q) protein was eluted with buffer H containing 2.5 mM biotin, and the eluate was dialyzed with PBS overnight.

In vitro cleavage fragment release assay

To generate 5' and internally radiolabeled target RNAs, synthesized 5' and 3' fragments of the target RNA were ^{32}P-radiolabeled at the 5' end using T4 polynucleotide kinase (Takara). After gel purification, the radiolabeled 5' fragment was ligated to a 5'-phosphorylated unlabeled 3' fragment, and the radiolabeled 3' fragment was ligated to an unlabeled 5' fragment by splinted ligation with T4 DNA ligase (NEB) at 30°C for 2 h, respectively. The radiolabeled target RNA was gel-purified and used for the assay. BmAgo3 immunoprecipitation for the cleavage assay was described previously (Izumi *et al*, 2022). A target cleavage assay was performed at 40°C for 2 h in a 10 μl reaction containing 3 μl of 40 × reaction mix (Haley *et al*, 2003) and 2 nM ^{32}P-radiolabeled target RNA. After the supernatant was removed, the BmAgo3-bound beads were further

incubated in buffer D containing 5 mM ATP and 350 nM recombinant proteins at 30°C for 1 h. Then, the supernatant and bead fractions were treated separately with proteinase K, and the target RNA was purified by EtOH precipitation. An image of the target RNA, separated on an 8% denaturing polyacrylamide gel, was captured using an FLA-7000 imaging system (Fujifilm Life Sciences). The oligonucleotides used for target RNA preparation are listed in Table EV1.

ATPase assay and thin layer chromatography

ATP hydrolysis reaction was performed at 25°C for 1 h using 2 μg of recombinant protein in buffer D containing 0.02% Triton X-100, 2 μM 36-nt polyU RNAs, and 0.23 μl of [γ-^{32}P] ATP (6000 Ci/mmol, Perkin Elmer). Twenty percent of the reaction mixture was spotted onto a polyethyleneimine cellulose plate (MACHEREY-NAGEL) that had been pre-run with water for 2 h. The plate was then run with 450 mM ammonium sulfate for 1 h, dried, and analyzed using an FLA-7000 imaging system (Fujifilm Life Sciences).

RNA extraction, northern blotting, and quantitative real-time PCR

For real-time PCR, northern blotting, and preparation of small RNA libraries, total RNA was prepared using TRI Reagent (Molecular Research Center) or the mirVana miRNA Isolation Kit (Thermo Fisher Scientific/Invitrogen). Northern blotting and quantitative real-time PCR were performed as described previously (Izumi *et al*, 2020). The probes for northern blotting and the primer sequences for real-time PCR are listed in Table EV1.

Immunofluorescence

BmN4 cells were fixed with 4% paraformaldehyde in PBS at room temperature for 10 min, then the cells were permeabilized with 0.3% Triton X-100 in PBS for 5 min. After pre-incubation with blocking buffer [PBS supplemented with 1% BSA (Merck Millipore/Sigma) and 0.1% Triton X-100] at room temperature for 1 h, the cells were incubated with primary antibodies [anti-FLAG antibody (M2; Merck Millipore/Sigma, 1/300), anti-HA antibody (3F10; Merck Millipore/Roche, 1/300), anti-Siwi antibody (1/400), anti-BmAgo3 antibody (1/300), anti-Spn-E antibody (1/250), or anti-DDX6 antibody (1/250)] in blocking buffer at 4□°C overnight. Alexa Fluor 488 donkey anti-mouse IgG, Alexa Fluor 488 donkey anti-rat IgG, Alexa Fluor 647 donkey anti-rabbit IgG, Alexa Fluor 647 goat anti-rat IgG, Dylight 488 goat anti-rabbit IgG, and Dylight 594 goat anti-mouse IgG secondary antibodies (Thermo Fisher Scientific) were used for detection. Biotinylated anti-BmAgo3 antibody was used after incubation with the secondary antibody, and the BmAgo3 signal was detected by Cy3-Streptavidin (Jackson ImmunoResearch). Images were captured using an Olympus FV3000 confocal laser scanning system with a × 60 oil immersion objective lens (PLAPON 60XO, NA 1.42; Olympus) and processed with FV31S-SW Viewer software and Adobe Photoshop Elements 10.

Mass spectrometry analysis

Immunoprecipitated BmAgo3 complexes separated by SDS-PAGE were stained with Coomassie brilliant blue (CBB), and the p160 band was excised from the gel, followed by in-gel digestion with trypsin (Promega) at 37°C for overnight. LC-MS/MS analysis was conducted using an LTQ-Orbitrap Velos mass spectrometer (Thermo Fisher Scientific) equipped with a nanoLC interface (Zaplous Advance nanoUHPLC HTS-PAL

xt System) (AMR). The nanoLC gradient was delivered at 500 nL/min and consisted of a linear gradient of mobile phase developed from 5 to 45% of acetonitrile in 60-180 min. Proteins were identified by the search algorithm Proteome Discoverer 2.4 (Thermo Fisher Scientific) using the protein database of *Bombyx mori* from NCBI.

Small RNA library preparation

Small RNA libraries were constructed from 20−50 nt total RNA according to the Zamore laboratory's open protocol (https://www.dropbox.com/s/r5d7aj3hhyaborq/) with some modifications (Fu *et al*, 2018). The 3′ adapter was conjugated with an amino CA linker instead of dCC at the 3′ end (GeneDesign) and adenylated using a 5′ DNA adenylation kit at the 5′ end (NEB). To reduce ligation bias, four random nucleotides were included in the 3′ and 5′ adapters [(5′-rAppNNNNTGGAATTCTCGGGTGCCAAGG/amino CA linker-3′) and (5′-GUUCAGAGUUCUACAGUCCGACGAUCNNNN-3′)] and adapter ligation was performed in the presence of 20% PEG-8000. After 3′ adapter ligation at 16°C for ≥16 h, the RNAs were size-selected by urea PAGE. For RNA extraction from a polyacrylamide gel, a ZR small-RNA PAGE Recovery Kit (ZYMO Research) was used. Small RNA libraries were sequenced on a HiSeq 4000 or DNBSEQ-G400 platform.

Sequence analysis of small RNA libraries

First, the adapter was removed by cutadapt using the sequence of the common part of the 3' adapter sequence after NNNN (Martin, 2011). The sequences were subsequently converted to fasta using fastq_to_fasta in the FASTX-Toolkit, and the completely duplicated sequences were removed using fastx_collapser to thin out to one (FASTX-

Toolkit; http://hannonlab.cshl.edu/fastx_toolkit/). Finally, Cutadapt was used to remove 4 nts of the UMI sequence from the 5' and 3' ends. Final sequences longer than 12 nt were used for analysis. Libraries were normalized by the number of reads that mapped to the genome allowing a single nucleotide mismatch by bowtie.

Mapping to transposons was performed using bowtie, allowing for a single nucleotide mismatch (Langmead *et al*, 2009). SAM files were converted to bam files by SAMtools (Li *et al*, 2009) and then to bed files by BEDTools (Quinlan & Hall, 2010). Among the mapped reads, reads between 23 and 32 nts in length were extracted as piRNAs using the awk command in Linux. The number of reads mapped to each transposon was measured using coverageBed in BEDtools, and the results were read into R to create a MAplot (Quinlan & Hall, 2010).

For individual piRNAs, mapping was performed with bowtie, allowing single nucleotide mismatches and multiple mapping to the surrounding regions of 3,236 previously constructed piRNA sequences (Izumi *et al*, 2016). SAM files were converted to bam files by SAMtools (Li *et al*, 2009) and then to bed files by BEDTools (Quinlan & Hall, 2010). Among the mapped reads, reads between 23 and 32 nts were extracted as piRNAs using the awk command in Linux. The results were used to obtain the position of the 5' end of the nearby piRNA for each piRNA using a custom script in R for subsequent analysis. Of the 3,236 piRNAs, 352 derived from TE1_bm_1645_LINE/R4, a transposon containing rRNA, were excluded from the analysis.

Definition of S→A, A→S, and S→S piRNAs

Only small RNA reads with 5'-end matches to the previously defined 3,236 piRNAs were extracted from the Siwi-IP and BmAgo3-IP libraries, and the IP libraries were

normalized by the total read count of the 3,236 piRNAs. Based on the RPM values, these piRNAs were then classified into Siwi-bound piRNAs and BmAgo3-bound piRNAs (i.e., “S” or “A” after the arrow) depending on whether they were more abundant in the Siwi-IP or the BmAgo3-IP library. Next, a similar analysis was performed on piRNAs with 5' 10-nt overlapping sequences to determine whether the ping-ping partner was Siwi or BmAgo3 (i.e., “S” or “A” before the arrow) based on their abundance in the IP libraries. The sequences of 352 rRNA-derived piRNAs, 212 piRNAs for which the PIWI protein bound to 5' 10-nt complementary piRNAs could not be determined (including many piRNAs that had no more than 1 read in the IP libraries), and 32 BmAgo3-bound piRNAs abundant in both the sense and antisense strands were excluded. Finally, 571 S→S piRNAs, 1,036 A→S piRNAs, and 1,033 S→A piRNAs were used for analysis.

Data availability

The sequencing data are deposited in the DDBJ database under accession numbers DRA017492–DRA017493 (https://ddbj.nig.ac.jp/resource/sra-submission/DRA017492, https://ddbj.nig.ac.jp/resource/sra-submission/DRA017493).

Acknowledgements

Illumina sequencing was performed by the Vincent J. Coates Genomics Sequencing Laboratory at UC Berkeley, supported by an NIH S10 OD018174 Instrumentation Grant. We thank all the members of the Tomari laboratory for critical comments on the manuscript. This work was supported in part by a Grant-in-Aid for Scientific Research

(S) (grant 18H05271 to Y.T.), a Grant-in-Aid for Scientific Research (A) (grant 23H00364 to Y.T.), a Grant-in-Aid for Scientific Research (C) (grant 23K05632 to N.I.) and a Grant-in-Aid for Early-Career Scientists (grant 22K15082 to K.S.).

Disclosure Statement and Competing Interests

The authors declare that they have no conflicts of interest.

References

Aravin AA, Heijden GW van der, Castañeda J, Vagin VV, Hannon GJ & Bortvin A (2009) Cytoplasmic Compartmentalization of the Fetal piRNA Pathway in Mice. *PLOS Genet* 5: e1000764

Aravin AA, Naumova NM, Tulin AV, Vagin VV, Rozovsky YM & Gvozdev VA (2001) Double-stranded RNA-mediated silencing of genomic tandem repeats and transposable elements in the *D. melanogaster* germline. *Curr Biol* 11: 1017–1027

Aravin AA, Sachidanandam R, Bourc'his D, Schaefer C, Pezic D, Toth KF, Bestor T & Hannon GJ (2008) A piRNA pathway primed by individual transposons is linked to de novo DNA methylation in mice. *Mol Cell* 31: 785–799

Brennecke J, Aravin AA, Stark A, Dus M, Kellis M, Sachidanandam R & Hannon GJ (2007) Discrete Small RNA-Generating Loci as Master Regulators of Transposon Activity in Drosophila. *Cell* 128: 1089–1103

Chen K, Yang X, Yang D & Huang Y (2023) Spindle-E is essential for gametogenesis in the silkworm, *Bombyx mori*. *Insect Sci* 30: 293–304

Choi S-Y, Huang P, Jenkins GM, Chan DC, Schiller J & Frohman MA (2006) A common lipid links Mfn-mediated mitochondrial fusion and SNARE-regulated exocytosis. *Nat Cell Biol* 8: 1255–1262

Chung PY, Shoji K, Izumi N & Tomari Y (2021) Dynamic subcellular compartmentalization ensures fidelity of piRNA biogenesis in silkworms. *EMBO Rep* 22: e51342

De Fazio S, Bartonicek N, Di Giacomo M, Abreu-Goodger C, Sankar A, Funaya C, Antony C, Moreira PN, Enright AJ & O'Carroll D (2011) The endonuclease activity of Mili fuels piRNA amplification that silences LINE1 elements. *Nature* 480: 259–263

Ding D, Liu J, Dong K, Midic U, Hess RA, Xie H, Demireva EY & Chen C (2017) PNLDC1 is essential for piRNA 3′ end trimming and transposon silencing during spermatogenesis in mice. *Nat Commun* 8: 819

Fu Y, Wu P-H, Beane T, Zamore PD & Weng Z (2018) Elimination of PCR duplicates in RNA-seq and small RNA-seq using unique molecular identifiers. *BMC Genomics* 19: 531

Gainetdinov I, Colpan C, Arif A, Cecchini K & Zamore PD (2018) A Single Mechanism of Biogenesis, Initiated and Directed by PIWI Proteins, Explains piRNA Production in Most Animals. *Mol Cell* 71: 775-790.e5

Ge DT, Wang W, Tipping C, Gainetdinov I, Weng Z & Zamore PD (2019) The RNA-Binding ATPase, Armitage, Couples piRNA Amplification in Nuage to Phased piRNA Production on Mitochondria. *Mol Cell* 74: 982-995.e6

Gillespie DE & Berg CA (1995) Homeless is required for RNA localization in Drosophila oogenesis and encodes a new member of the DE-H family of RNA-dependent ATPases. *Genes Dev* 9: 2495–2508

Gunawardane LS, Saito K, Nishida KM, Miyoshi K, Kawamura Y, Nagami T, Siomi H & Siomi MC (2007) A Slicer-Mediated Mechanism for Repeat-Associated siRNA 5' End Formation in Drosophila. *Science* 315: 1587–1590

Haley B, Tang G & Zamore PD (2003) In vitro analysis of RNA interference in *Drosophila melanogaster*. *Methods* 30: 330–336

Han BW, Wang W, Li C, Weng Z & Zamore PD (2015) piRNA-Guided Transposon Cleavage Initiljates Zucchini-Dependent, Phased piRNA Production. *Science* 348: 817

Horwich MD, Li C, Matranga C, Vagin V, Farley G, Wang P & Zamore PD (2007) The Drosophila RNA Methyltransferase, DmHen1, Modifies Germline piRNAs and Single-Stranded siRNAs in RISC. *Curr Biol* 17: 1265–1272

Hutvagner G & Simard MJ (2008) Argonaute proteins: key players in RNA silencing. *Nat Rev Mol Cell Biol* 9: 22–32

Izumi N, Shoji K, Kiuchi T, Katsuma S & Tomari Y (2022) The two Gtsf paralogs in silkworms orthogonally activate their partner PIWI proteins for target cleavage. *RNA* 29: 18–29

Izumi N, Shoji K, Sakaguchi Y, Honda S, Kirino Y, Suzuki T, Katsuma S & Tomari Y (2016) Identification and Functional Analysis of the Pre-piRNA 3' Trimmer in Silkworms. *Cell* 164: 962–973

Izumi N, Shoji K, Suzuki Y, Katsuma S & Tomari Y (2020) Zucchini consensus motifs determine the mechanism of pre-piRNA production. *Nature* 578: 311–316

Kawaoka S, Hayashi N, Suzuki Y, Abe H, Sugano S, Tomari Y, Shimada T & Katsuma S (2009) The Bombyx ovary-derived cell line endogenously expresses PIWI/PIWI-interacting RNA complexes. *RNA* 15: 1258–1264

Kirino Y & Mourelatos Z (2007) The mouse homolog of HEN1 is a potential methylase for Piwi-interacting RNAs. *RNA* 13: 1397–1401

Kuramochi-Miyagawa S, Watanabe T, Gotoh K, Totoki Y, Toyoda A, Ikawa M, Asada N, Kojima K, Yamaguchi Y, Ijiri TW, *et al* (2008) DNA methylation of retrotransposon genes is regulated by Piwi family members MILI and MIWI2 in murine fetal testes. *Genes Dev* 22: 908–917

Langmead B, Trapnell C, Pop M & Salzberg SL (2009) Ultrafast and memory-efficient alignment of short DNA sequences to the human genome. *Genome Biol* 10: R25

Li H, Handsaker B, Wysoker A, Fennell T, Ruan J, Homer N, Marth G, Abecasis G & Durbin R (2009) The Sequence Alignment/Map format and SAMtools. *Bioinformatics* 25: 2078–2079

Lim AK & Kai T (2007) Unique germ-line organelle, nuage, functions to repress selfish genetic elements in *Drosophila melanogaster*. *Proc Natl Acad Sci USA* 104: 6714–6719

Malone CD, Brennecke J, Dus M, Stark A, McCombie WR, Sachidanandam R & Hannon GJ (2009) Specialized piRNA Pathways Act in Germline and Somatic Tissues of the Drosophila Ovary. *Cell* 137: 522–535

Martin M (2011) Cutadapt removes adapter sequences from high-throughput sequencing reads. *EMBnet.journal* 17: 10–12

Mohn F, Handler D & Brennecke J (2015) Noncoding RNA. piRNA-guided slicing specifies transcripts for Zucchini-dependent, phased piRNA biogenesis. *Science* 348: 812–817

Murakami R, Sumiyoshi T, Negishi L & Siomi MC (2021) DEAD-box polypeptide 43 facilitates piRNA amplification by actively liberating RNA from Ago3-piRISC. *EMBO Rep* 22: e51313

Namba Y, Iwasaki YW, Nishida KM, Nishihara H, Sumiyoshi T & Siomi MC (2022) Maelstrom functions in the production of Siwi-piRISC capable of regulating transposons in Bombyx germ cells. *iScience* 25: 103914

Nishida KM, Iwasaki YW, Murota Y, Nagao A, Mannen T, Kato Y, Siomi H & Siomi MC (2015) Respective functions of two distinct Siwi complexes assembled during PIWI-interacting RNA biogenesis in Bombyx germ cells. *Cell Rep* 10: 193–203

Nishida KM, Sakakibara K, Sumiyoshi T, Yamazaki H, Mannen T, Kawamura T, Kodama T & Siomi MC (2020) Siwi levels reversibly regulate secondary piRISC biogenesis by affecting Ago3 body morphology in *Bombyx mori*. *EMBO J* 39: e105130

Nishimura T, Nagamori I, Nakatani T, Izumi N, Tomari Y, Kuramochi-Miyagawa S & Nakano T (2018) PNLDC1, mouse pre-piRNA Trimmer, is required for meiotic and post-meiotic male germ cell development. *EMBO Rep* 19: e44957

Ott KM, Nguyen T & Navarro C (2014) The DExH box helicase domain of spindle-E is necessary for retrotransposon silencing and axial patterning during Drosophila oogenesis. *G3 (Bethesda)* 4: 2247–2257

Ozata DM, Gainetdinov I, Zoch A, O'Carroll D & Zamore PD (2019) PIWI-interacting RNAs: small RNAs with big functions. *Nat Rev Genet* 20: 89–108

Patil AA, Tatsuke T, Mon H, Lee JM, Morokuma D, Hino M & Kusakabe T (2017) Molecular characterization of mitochondrial Zucchini and its relation to nuage-piRNA pathway components in *Bombyx mori* ovary-derived BmN4 cells. *Biochem Biophys Res Commun* 493: 971–978

Quinlan AR & Hall IM (2010) BEDTools: a flexible suite of utilities for comparing genomic features. *Bioinformatics* 26: 841–842

Reuter M, Berninger P, Chuma S, Shah H, Hosokawa M, Funaya C, Antony C, Sachidanandam R & Pillai RS (2011) Miwi catalysis is required for piRNA amplification-independent LINE1 transposon silencing. *Nature* 480: 264–267

Saito K, Ishizu H, Komai M, Kotani H, Kawamura Y, Nishida KM, Siomi H & Siomi MC (2010) Roles for the Yb body components Armitage and Yb in primary piRNA biogenesis in Drosophila. *Genes Dev* 24: 2493–2498

Saito K, Sakaguchi Y, Suzuki T, Suzuki T, Siomi H & Siomi MC (2007) Pimet, the Drosophila homolog of HEN1, mediates 2′-O-methylation of Piwi- interacting RNAs at their 3′ ends. *Genes Dev* 21: 1603–1608

Shoji M, Tanaka T, Hosokawa M, Reuter M, Stark A, Kato Y, Kondoh G, Okawa K, Chujo T, Suzuki T, *et al* (2009) The TDRD9-MIWI2 complex is essential for

piRNA-mediated retrotransposon silencing in the mouse male germline. *Dev Cell* 17: 775–787

Sienski G, Dönertas D & Brennecke J (2012) Transcriptional silencing of transposons by Piwi and maelstrom and its impact on chromatin state and gene expression. *Cell* 151: 964–980

Siomi MC, Mannen T & Siomi H (2010) How does the Royal Family of Tudor rule the PIWI-interacting RNA pathway? *Genes Dev* 24: 636–646

Standart N & Weil D (2018) P-Bodies: Cytosolic Droplets for Coordinated mRNA Storage. *Trends in Genetics* 34: 612–626

Stapleton W, Das S & McKee BD (2001) A role of the Drosophila homeless gene in repression of Stellate in male meiosis. *Chromosoma* 110: 228–240

Vagin VV, Sigova A, Li C, Seitz H, Gvozdev V & Zamore PD (2006) A Distinct Small RNA Pathway Silences Selfish Genetic Elements in the Germline. *Science* 313: 320–324

Wang W, Yoshikawa M, Han BW, Izumi N, Tomari Y, Weng Z & Zamore PD (2014) The Initial Uridine of Primary piRNAs Does Not Create the Tenth Adenine that Is the Hallmark of Secondary piRNAs. *Mol Cell* 56: 708–716

Wang X, Ramat A, Simonelig M & Liu M-F (2023) Emerging roles and functional mechanisms of PIWI-interacting RNAs. *Nat Rev Mol Cell Biol* 24: 123–141

Wenda JM, Homolka D, Yang Z, Spinelli P, Sachidanandam R, Pandey RR & Pillai RS (2017) Distinct Roles of RNA Helicases MVH and TDRD9 in PIWI Slicing-Triggered Mammalian piRNA Biogenesis and Function. *Dev Cell* 41: 623-637.e9

Xiol J, Spinelli P, Laussmann MA, Homolka D, Yang Z, Cora E, Couté Y, Conn S, Kadlec J, Sachidanandam R, *et al* (2014) RNA clamping by Vasa assembles a piRNA amplifier complex on transposon transcripts. *Cell* 157: 1698–1711

Zhang Y, Guo R, Cui Y, Zhu Z, Zhang Y, Wu H, Zheng B, Yue Q, Bai S, Zeng W, *et al* (2017) An essential role for PNLDC1 in piRNA 3′ end trimming and male fertility in mice. *Cell Res* 27: 1392–1396

Zhang Z, Xu J, Koppetsch BS, Wang J, Tipping C, Ma S, Weng Z, Theurkauf WE & Zamore PD (2011) Heterotypic piRNA Ping-Pong requires qin, a protein with both E3 ligase and Tudor domains. *Mol Cell* 44: 572–584

Figure Legends

Fig 1. The ATPase-deficient Spn-E-EQ forms aggregates with BmAgo3.

A CBB staining of immunoprecipitated BmAgo3 complexes from BmN4 cells treated with dsRNA targeting *Rluc* or *Siwi*. *Rluc*; *Renilla luciferase*, control. HC; IgG heavy chain, LC; IgG light chain.

B Subcellular localization of BmAgo3, Spn-E, and FLAG-DDX43 in BmN4 cells treated with dsRNA targeting *Rluc* or *Siwi*. *Rluc*; *Renilla luciferase*, control. Scale bar, 5 μm.

C Subcellular localization of FLAG-Spn-E (wild type or EQ) and BmAgo3 in BmN4 cells treated with dsRNA targeting the *Spn-E* 3' UTR. Scale bar, 5 μm.

D Western blot analysis of immunopurified FLAG-Spn-E (wild type or EQ) complexes from BmN4 cells treated with dsRNA targeting the *Spn-E* 3' UTR. Quantification data from three independent experiments are shown in Fig EV1A.

E Northern blot analysis of piR1712, piR2986, and piR484 in BmN4 cells co-transfected with the FLAG-Spn-E (wild type or EQ) plasmid and dsRNA targeting the *Spn-E* 3' UTR. Quantification data for mature piRNA and pre-piRNA signals from four independent experiments are shown in Fig EV1F and G, respectively.

Fig 2. Depletion of Spn-E decreases BmAgo3-dependent production of Siwi-bound piRNAs while increasing Siwi-Siwi homotypic ping-pong.

A MA plot showing piRNA expression changes between control KD (*Rluc* RNAi) and *Spn-E* KD using dsRNA targeting the *Spn-E* 3' UTR. Each dot represents one piRNA. Based on the changes in expression, piRNAs were divided into three groups:

"increased" (red, n = 825), "unchanged" (green, n = 824), and "decreased" (blue, n = 825).

B Relative fractions of 1U10A, 1U but not 10A, 10A but not 1U, and neither 1U nor 10A piRNAs of each group defined in (A).

C Schematic representation of A→S, S→A, and S→S piRNAs.

D Changes in the expression of A→S, S→A, and S→S piRNAs in *Spn-E* KD relative to control KD (*Rluc* RNAi). Two different dsRNAs targeting the *Spn-E* CDS and 3' UTR were used.

E Changes in the expression of A→S, S→A, and S→S piRNAs in the indicated conditions relative to control KD (*Rluc* RNAi). The *Spn-E* RNAi (UTR) data in (D) are included for comparison.

F Summary of the results from the *Spn-E* KD rescue experiment. *Spn-E* KD decreases A→S piRNAs and increases S→S piRNAs. A→S piRNA production requires the ATPase activity of Spn-E, whereas the suppression of S→S piRNA production does not.

Fig 3. Artificial Siwi-bound piRNA production is impaired by Spn-E KD but not by DDX43 KD.

A Schematic representation of the piR484-A reporter. piR484-A is an artificial A→S piRNA with a chimeric sequence of piR484 and piR2986. The details are shown in Fig EV3A.

B Siwi was immunoprecipitated from BmN4 cells co-transfected with the piR484-A reporter plasmid and dsRNA targeting the indicated genes for RNAi. Immunoprecipitated Siwi and Siwi-bound piR484-A were detected by western blotting

and northern blotting, respectively. *Rluc*; *Renilla luciferase*, control.

C Schematic representation of the production of *piggyBac* piRNA reporter-derived artificial Siwi-bound piRNAs. (Left) The circular plasmid produces a reporter RNA with a long 3' region. After cleavage by *piggyBac* piRNA-loaded BmAgo3, the 3' end of the Siwi-loaded reporter RNA is processed by an unknown downstream cleavage event and/or trimming by Trimmer. (Right) After cleavage by *piggyBac* piRNA-loaded BmAgo3, the reporter RNA from the linearized plasmid is expected to be 30 nt long, which is similar in length to that of endogenous piRNAs. Consequently, additional 3' end processing is unnecessary in theory.

D Siwi was immunoprecipitated from BmN4 cells co-transfected with a circular or linearized *piggyBac* piRNA reporter plasmid and dsRNA targeting the indicated genes for RNAi. Immunoprecipitated Siwi and reporter-derived artificial Siwi-bound piRNAs (art-Siwi piRNAs) were detected by western blotting and northern blotting, respectively. *Rluc*; *Renilla luciferase*, control.

E KD rescue experiment of Spn-E using the *piggyBac* piRNA reporter. Siwi was immunoprecipitated from BmN4 cells co-transfected with a circular *piggyBac* piRNA reporter plasmid, the FLAG-Spn-E expression plasmid, and dsRNA targeting the *Spn-E* 3' UTR. Immunoprecipitated Siwi and reporter-derived artificial Siwi-bound piRNAs (art-Siwi piRNAs) were detected by western blotting and northern blotting, respectively. *Rluc*; *Renilla luciferase*, control.

Expanded View Figure Legends

Fig EV1. Characterization of Spn-E-EQ aggregates and BmAgo3 cleavage fragment release assay.

A Quantification of Siwi and BmAgo3 signals co-immunoprecipitated with FLAG-Spn-E (wild type or EQ) in Fig 1D. Relative co-immunoprecipitated levels normalized to the Spn-E IP level are shown. Data are mean ± s.d. of three independent experiments (biological replicates). Statistical analysis was performed using a two-sided Student's paired t-test, with *p*-values adjusted using the Holm method. NS, not significant.

B Western blot analysis of whole cell lysates of BmN4 cells treated with dsRNA for *Rluc* (control) or *DDX6*. The anti-DDX6 antibody successfully detected endogenous DDX6.

C Subcellular localization of FLAG-Spn-E-EQ, DDX6, a P-body marker protein, and BmAgo3 in BmN4 cells. Scale bar, 5 μm.

D Subcellular localization of FLAG-Spn-E-EQ, BmAgo3 and Siwi in BmN4 cells. Scale bar, 5 μm.

E Tandem IP experiment on BmN4 cells co-transfected with the FLAG-Spn-E-EQ expression plasmid and dsRNA targeting the *Spn-E* 3' UTR. FLAG-Spn-E-EQ was first immunoprecipitated with the FLAG tag, and the resulting immunopurified complex was then subjected to a second IP with normal rabbit IgG (Contl-IgG) or an anti-BmAgo3 antibody. Siwi in the second immunoprecipitate was detected by western blotting with or without RNase A treatment.

F Quantification of mature piRNA signals in Fig 1E. Relative expression levels

normalized to those under Spn-E WT expression are shown. Data are mean ± s.d. of four independent experiments (biological replicates). Statistical analysis was performed using a two-sided Student's paired t-test, with *p*-values adjusted using the Holm method (*p = 0.023).

G Quantification of pre-piRNA signals in Fig 1E. Relative expression levels normalized to those under Spn-E WT expression are shown. Data are mean ± s.d. of four independent experiments (biological replicates). Statistical analysis was performed using a two-sided Student's paired t-test, with *p*-values adjusted using the Holm method (*p = 0.025, **p = 0.003).

H CBB staining of purified recombinant Spn-E and DDX43 proteins (rSpn-E and rDDX43, indicated by arrowheads) used for the in vitro cleavage fragment release assay.

I (Top) Schematic representation of the in vitro cleavage fragment release assay. To detect cleaved 5' and 3' fragments separately, the target RNA was radiolabeled at different positions (*). The 5' or internally radiolabeled target RNAs were subjected to a cleavage assay using BmAgo3 immunoprecipitates. After the reaction, the bead fraction was incubated with rSpn-E or rDDX43 in the presence of ATP. (Bottom) The cleaved fragments in the supernatant and bead fractions were detected by autoradiography.

J Thin-layer chromatography for the detection of ATPase activity of the recombinant Spn-E protein.

K Subcellular localization of FLAG-DDX43 (wild type or DA, an ATPase-deficient mutant) and BmAgo3 in BmN4 cells. Scale bar, 5 μm.

L Subcellular localization of FLAG-Spn-E-EQ, HA-DDX43, and BmAgo3 in BmN4 cells. Scale bar, 5 μm.

Fig EV2. Changes in the expression of TE-mapped piRNAs upon KD of *Spn-E* or *DDX43*.

A Western blot analysis of whole cell lysates from BmN4 cells treated with dsRNA for *Rluc* (control), *Spn-E*, or *DDX43*. Two different dsRNAs (*Spn-E*: CDS and 3' UTR; *DDX43*: two different regions of the CDS, #1 and #2) were used for RNAi. *Rluc*; *Renilla luciferase*.

B Quantitative real-time PCR analysis of the expression of *DDX43* in BmN4 cells treated with dsRNA for *Rluc* (control), *Spn-E*, or *DDX43*. Relative mRNA expression levels normalized to those of *rp49* are shown. *Rluc*; *Renilla luciferase*.

C MA plots showing piRNA expression changes for each TE between the control KD (*Rluc* RNAi) and *Spn-E* or *DDX43* KD. Two different dsRNAs (CDS and 3' UTR) were used for *Spn-E* RNAi. Each dot represents one TE. TEs with increased piRNA production in the *Spn-E* RNAi (UTR) are colored red.

D MA plot showing piRNA expression changes between the control KD (*Rluc* RNAi) and *Spn-E* KD using dsRNA targeting the *Spn-E* CDS. Each dot represents one piRNA. Based on the three groups defined in Fig 2A, piRNAs were color-coded as follows: “increased” (red, n = 825), “unchanged” (green, n = 824), and “decreased” (blue, n = 825).

E MA plot showing piRNA expression changes between control KD (*Rluc* RNAi) and *Spn-E* KD using dsRNA targeting the *Spn-E* CDS. Each dot represents one piRNA. Based on the changes in expression, piRNAs were divided into three groups: “increased” (red, n = 805), “unchanged” (green, n = 805), and “decreased” (blue, n = 805).

F Relative fractions of 1U10A, 1U but not 10A, 10A but not 1U, and neither 1U nor 10A piRNAs of each group in (E).

G Scatter plots showing the PIWI binding bias of 1U but not 10A, 10A but not 1U, or 1U10A piRNAs (x-axis) and that of their putative partner piRNAs in the ping-pong cycle (y-axis).

H Changes in the expression of A→S, S→A, and S→S piRNAs in *DDX43* KD relative to control KD (*Rluc* RNAi). Two different dsRNAs targeting the *DDX43* CDS were used for RNAi. *Rluc*; *Renilla luciferase*.

Fig EV3. Construction of the piR484-A reporter system and Spn-E KD rescue experiment using the piR484-A reporter.

A Schematic explanation of the construction of the piR484-A reporter. piR484 is an S→A piRNA, and the sequence including the 5' 10 nt and the upstream region of piR484 was replaced with the corresponding region of piR2986, an A→S piRNA, resulting in an artificial A→S piRNA, piR484-A. The downstream sequence of piR484 that contains a Siwi-bound piRNA target sequence was used without modification.

B Quantitative real-time PCR analysis of the expression of *DDX43* in the reporter experiments in Fig 3B and 3D. Relative mRNA expression levels normalized to those of *rp49* are shown. *Rluc*; *Renilla luciferase*, control.

C KD rescue experiment of Spn-E using the piR484-A reporter. Siwi was immunoprecipitated from BmN4 cells co-transfected with the piR484-A reporter plasmid, the FLAG-Spn-E expression plasmid, and dsRNA targeting the *Spn-E* 3' UTR. Immunoprecipitated Siwi and Siwi-bound piR484-A were detected by western blotting and northern blotting, respectively. *Rluc*; *Renilla luciferase*, control.

Figure 1

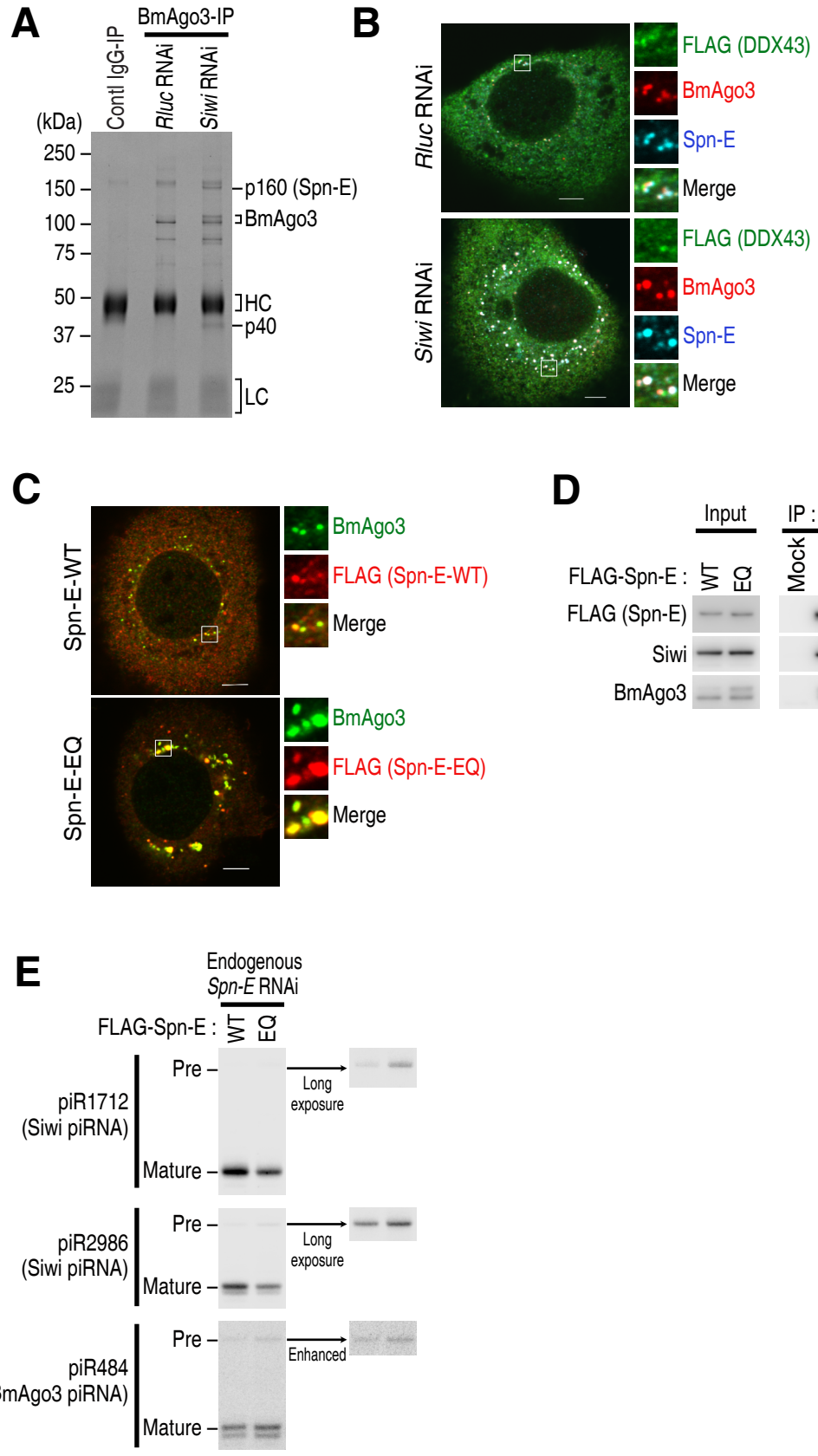

Figure 2

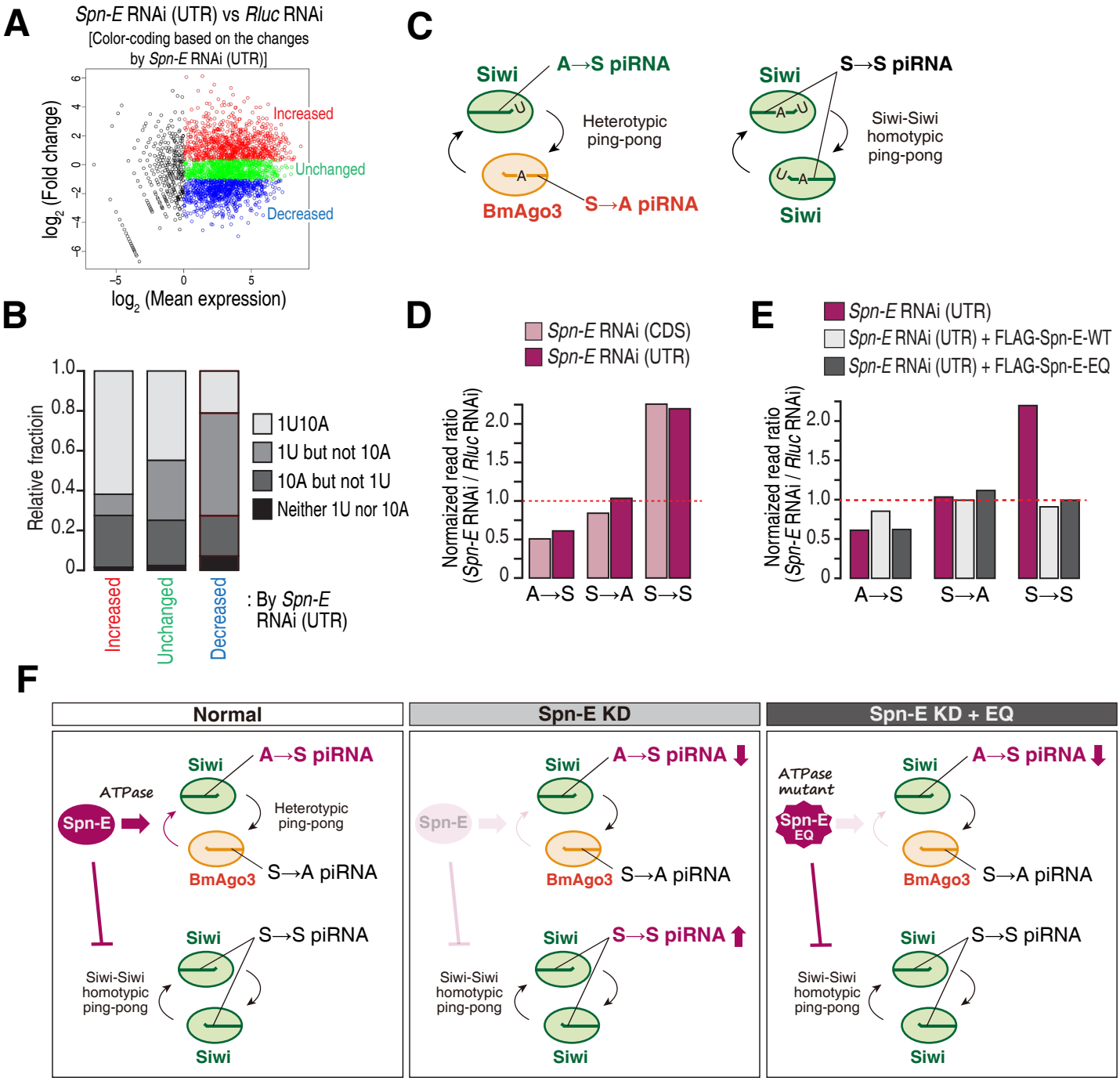

Figure 3